amplitudes are consistent for acid quenching and diazonium salt quenching, and Auger quenching of excitons is known to be efficient.

Is the exciton motion ballistic or diffusional? For the bright emissive SWNTs studied here, we assume an exciton recombination lifetime τ = 100 ps, which is among the larger values reported from time-resolved spectroscopy (*24*, *25*), If the motion is ballistic, then the exciton's kinetic energy would be given by

$$E_{\text{ballistic}} = \frac{1}{2} m^*_{\text{exciton}} \left(\frac{\Lambda}{\tau}\right)^2 \quad (1)$$

where m^*_{exciton} is the exciton effective mass. Using an estimated m^*_{exciton} of ~$0.1m_e$ (*1*, *26*), we obtain $E_{\text{ballistic}} \sim 10^{-7}$ eV. This value is orders of magnitude lower than the 0.012 eV ($\frac{1}{2}k_BT$) expected from rapid thermalization induced by the exciton-phonon coupling evident in SWNT spectroscopy (*27*). We conclude that the excitonic motion is instead diffusional, in agreement with a recent investigation on bulk samples (*28*). The corresponding diffusion coefficient for the exciton one-dimensional random walk is then given as $D = \Lambda^2/2\tau \sim 0.4$ cm^2 s^{-1}.

This value lies more than two orders of magnitude below a prior tentative estimate that was indirectly deduced from transient absorption experiments on ensembles of short SWNTs in annealed dried films (*29*). The exciton diffusion coefficient measured here for highly luminescent individual SWNTs may be used to interpret the ~150 cm^{-1} Lorentzian line widths observed in emission spectroscopy of room-temperature SWNTs (see Figs. 1B and 2B). These widths arise from dephasing that is far more rapid (70 fs) than the ~100-ps exciton population lifetime τ.

If dephasing instead occurs by diffusional hopping of the exciton along the tube axis, then the hopping step length d_{hop} can be estimated from the relation $D = d_{\text{hop}}^2/2\tau_{\text{hop}}$, where τ_{hop} represents the interval between hops, identified as the 70-fs dephasing time. This approach gives a hopping step length of ~2 nm, which closely matches theoretical estimates of the exciton size (*1*–*3*). We propose that the emission linewidth may originate from thermally assisted short-range hopping of excitons along the nanotube axis. At cryogenic temperatures, suppression of this hopping would then remove the major source of line broadening and would account for markedly narrower spectral features (*30*).

If efficient exciton quenching occurs not only at chemical derivatization sites but also at the ends of cut nanotubes, our value of the exciton diffusion range Λ naturally explains the strong reduction in PL reported for SWNTs shorter than ~100 nm (*31*). More generally, the measured diffusion range implies that one exciton will visit ~10^4 carbon atoms during its lifetime. Thus, PL becomes remarkably sensitive to certain sidewall electronic perturbations, which may include chemical derivatizations and defects introduced during nanotube processing. PL may then prove useful for detecting local pH gradients in restricted environments, such as microfluidic channels or organelles inside biological cells.

References and Notes

1. T. G. Pedersen, *Phys. Rev. B* **67**, 073401 (2003).
2. V. Perebeinos, J. Tersoff, Ph. Avouris, *Phys. Rev. Lett.* **92**, 257402 (2004).
3. C. D. Spataru *et al.*, *Phys. Rev. Lett.* **92**, 077402 (2004).
4. J. Chen *et al.*, *Science* **310**, 1171 (2005).
5. Y.-Z. Ma *et al.*, *Phys. Rev. Lett.* **94**, 157402 (2005).
6. F. Wang *et al.*, *Phys. Rev. B* **70**, 241403R (2004).
7. M. O'Connell *et al.*, *Science* **297**, 593 (2002).
8. M. S. Strano *et al.*, *J. Phys. Chem. B* **107**, 6979 (2003).
9. M. L. Usrey, E. S. Lippmann, M. S. Strano, *J. Am. Chem. Soc.* **127**, 16129 (2005).
10. W. E. Moerner, M. Orrit, *Science* **283**, 1670 (1999).
11. L. Cognet *et al.*, *Sci. STKE* **2006**, pe13 (2006).
12. A. Hartschuh *et al.*, *Science* **301**, 1354 (2003).
13. J. Lefebvre *et al.*, *Phys. Rev. B* **69**, 075403 (2004).
14. D. A. Tsyboulski, S. M. Bachilo, R. B. Weisman, *Nano Lett.* **5**, 975 (2005).
15. See supporting material on *Science* Online.
16. R. M. Dickson *et al.*, *Science* **274**, 966 (1996).
17. S. M. Bachilo *et al.*, *Science* **298**, 2361 (2002).
18. G. Dukovic *et al.*, *J. Am. Chem. Soc.* **126**, 15269 (2004).
19. M. S. Strano *et al.*, *Science* **301**, 1519 (2003).
20. J. L. Bahr *et al.*, *J. Am. Chem. Soc.* **123**, 6536 (2001).
21. C. A. Dyke *et al.*, *Synlett* **2004**, 155 (2004).
22. D. Bonifazi *et al.*, *Nano Lett.* **6**, 1408 (2006).
23. The studied SWNT species were (7,3), (7,5), (7,6), (8,3), (8,6), (9,5), (9,7), (10,5), (12,1), (11,1), and (11,3).
24. A. Hagen *et al.*, *Phys. Rev. Lett.* **95**, 197401 (2005).
25. M. Jones *et al.*, *Nano Lett.* **7**, 300 (2007).
26. C. D. Spataru *et al.*, *Phys. Rev. Lett.* **95**, 247402 (2005).
27. M. S. Dresselhaus, G. Dresselhaus, Ph. Avouris, *Carbon Nanotubes: Synthesis, Structure, Properties, and Applications* (Springer-Verlag, New York, 2001).
28. R. M. Russo *et al.*, *Phys. Rev. B* **74**, 041405 (2006).
29. O. J. Korovyanko *et al.*, *Phys. Rev. Lett.* **92**, 017403 (2004).
30. H. Htoon *et al.*, *Phys. Rev. Lett.* **93**, 027401 (2004).
31. D. A. Heller *et al.*, *J. Am. Chem. Soc.* **126**, 14567 (2004).

32. Supported by the Fulbright Foundation and Delegation Generale pour l'Armement (DGA) grant ERE060016 (L.C.), Welch Foundation postdoctoral fellowship L-C-0004 (D.A.T.), the Rice-Houston Alliances for Graduate Education in the Professoriate (AGEP) program (NSF Cooperative HRD-0450363) (J.D.R.R.), NSF grant CHE-0314270, NSF Center for Biological and Environmental Nanotechnology grant EEC-0647452, Welch Foundation grant C-0807, NASA grant JSC-NNJ06HC25G, and Applied NanoFluorescence LLC. We thank J. T. Willerson, S. W. Casscells III, and J. L. Conyers for instrumentation support.

Supporting Online Material

www.sciencemag.org/cgi/content/full/316/5830/1465/DC1
Materials and Methods
Figs. S1 to S2
Movie S1
References

14 February 2007; accepted 23 April 2007
10.1126/science.1141316

Seismic Evidence for Deep-Water Transportation in the Mantle

Hitoshi Kawakatsu* and Shingo Watada

We report seismic evidence for the transportation of water into the deep mantle in the subduction zone beneath northeastern Japan. Our data indicate that water is released from the hydrated oceanic crust at shallow depths (≲100 kilometers) and then forms a channel of hydrated mantle material on top of the subducting plate that is the pathway for water into the deep mantle. Our result provides direct evidence that shows how water is transported from the ocean to the deep mantle in a cold subduction zone environment.

Water in the mantle is expected to play essential roles in various notable problems of geodynamics, such as the generation of arc volcanism (*1*), lubrication of the subduction zone plate interface that may trigger large earthquakes (*2*), and control of mantle rheology (*3*). How water is transported into the mantle, however, has not been clear, except that it is generally believed that subducting hydrated oceanic crust is the major carrier, preventing Earth scientists from accurately estimating the overall water circulation budget of the Earth system (*4*).

Beneath northeastern Japan, the old Pacific plate is subducting along the Japan trench. Owing partly to the favorable subduction geometry, as well as the dense and well-maintained seismic network there, it is the most detail-studied subduction zone on the planet, and a number of discoveries of subduction processes have been made there. In recent years, these have included the finding of a double seismic zone (*5*); detailed mapping of a low-velocity area in the mantle wedge that possibly corresponds to a pathway of magmatic melt migration responsible for arc volcanism (*6*–*8*); fingerlike distribution of active volcanoes (*9*, *10*); and a transition from the trench-parallel to trench-normal seismic anisotropy (*11*). On the basis of these findings, we now have a much better understanding of the detailed mechanics of subduction. However, if we consider a subduction zone as a place of material consumption (subduction of the oceanic plate)

Earthquake Research Institute, University of Tokyo, 1-1-1 Yayoi, Bunkyo-ku, Tokyo 113-0032, Japan.

*To whom correspondence should be addressed. E-mail: hitosi@eri.u-tokyo.ac.jp

and production (generation of arc volcanism), understanding of the essential element—how water is transported into the mantle—is still not resolved.

Water exists in oceanic crust as various hydrous minerals. When the oceanic plate subducts at the trench, the hydrated crust carries water with it in the form of hydrous meta-basalt [e.g., blueschist (*12*)]. The presence of hydrous minerals in the oceanic crust reduces the seismic velocity to considerably less than the velocity of the surrounding mantle (*13*, *14*), and evidence for this has been detected in different subduction environments as a low-velocity layer near the top surface of the subducting plate (*15*, *16*). It is experimentally established that those hydrous minerals become unstable at pressure and temperature conditions characteristic of a shallow subduction zone (~50-km depth) and are dehydrated to become anhydrous eclogitic oceanic crust. This dehydration process is expected to occur at depths of ~50 to ~150 km in a cold subduction environment such as exists beneath northeast Japan (*14*, *17*), and expelled free water should move directly upward due to buoyancy into the mantle wedge. Because the presence of water substantially lowers the melting temperature of the mantle peridotite, it is generally believed that this water eventually triggers the mantle melting to generate island arc volcanism (*1*). What is not resolved is how and where this process occurs in the mantle wedge.

On the basis of seismic tomography and a numerical simulation, Iwamori and Zhao (*17*) suggested that free water in the mantle wedge metamorphoses (or hydrates) the mantle peridotite into hydrous serpentinite, and the serpentinized mantle is dragged downward parallel to the direction of the slab subduction, forming a thin serpentinite layer along the top surface of the subducting slab. The postulated serpentinite layer may be the pathway by which substantial amounts of water are transported into the deep mantle (*4*). It is, however, difficult to resolve the existence of such a layer by seismic transmission tomography, owing to the low sensitivity of this method. The scattered seismic wavefield, by contrast, is sensitive to local velocity changes and thus has the potential to resolve thin layers.

We reconstructed such a scattered seismic wave field to image the reflectivity profile beneath northeast Japan (Fig. 1). We used the receiver function (RF) technique (*18*–*20*) and obtained the data from the Japanese Hi-net seismic array (*21*) [see Supporting Online Material (SOM)]. The RF images (Fig. 1 and fig. S1) show clear images of the top part of the subducting Pacific plate: The oceanic Moho is mapped continuously parallel to the upper plane of the double seismic zone (*5*) as positive RFs (red in the figure, representing the velocity increase with depth). Above this feature, a strong velocity decrease (negative RFs, blue), due to the presence of the hydrous oceanic crust, is observed. The strength of the negative RFs is reduced drastically at depths of 50 to 90 km (Fig. 2), where the hydrous minerals are expected to dehydrate. The seismic velocity of the hydrous oceanic crust is much slower than that of the surrounding mantle, whereas that of the anhydrous eclogitic crust is seismically indistinguishable (*13*). Thus, the degree of dehydration would strongly control the reflectivity at the top part of the slab, and our images are in good agreement with existing models of the oceanic crust dehydration (*14*, *17*). We therefore conclude that this reduction of the RF amplitudes provides direct evidence for the dehydration of subducted oceanic crust at this depth range.

At a depth of ~90 km, where strong negative RFs disappear, positive RFs emerge parallel to the dip of the subducting plate (pink line in Fig. 1B). Because the positive RF corresponding to the oceanic Moho (red line) continues to just below this feature, it cannot be the oceanic Moho itself displaced upward due to the effect of some unmodeled structure. A positive RF is a signature of a velocity increase, and thus the observed feature indicates that the seismic velocity is slower above the top of the subducting plate. The similarity between our RF image and the numerically predicted water content in the mantle wedge (Fig. 3A) allows us to interpret the image as follows (Fig. 3B): The dehydration of the oceanic crust causes its velocity to increase, whereas the serpentinization of the mantle wedge peridotite by the expelled water causes the velocity there to decrease. As this process continues to deep subduction, there is a depth at which the seismic velocity of serpentinized mantle wedge becomes slower than that of the oceanic crust underneath; below this depth, both the top and bottom sides of the oceanic crust show a velocity increase with depth and are imaged as positive RFs, as observed in Fig. 1A. The top part of the serpentinized low-velocity layer is not imaged in Fig. 1A, possibly reflecting a more gradual boundary due to the diffusive nature of the hydration/dehydration process (*22*).

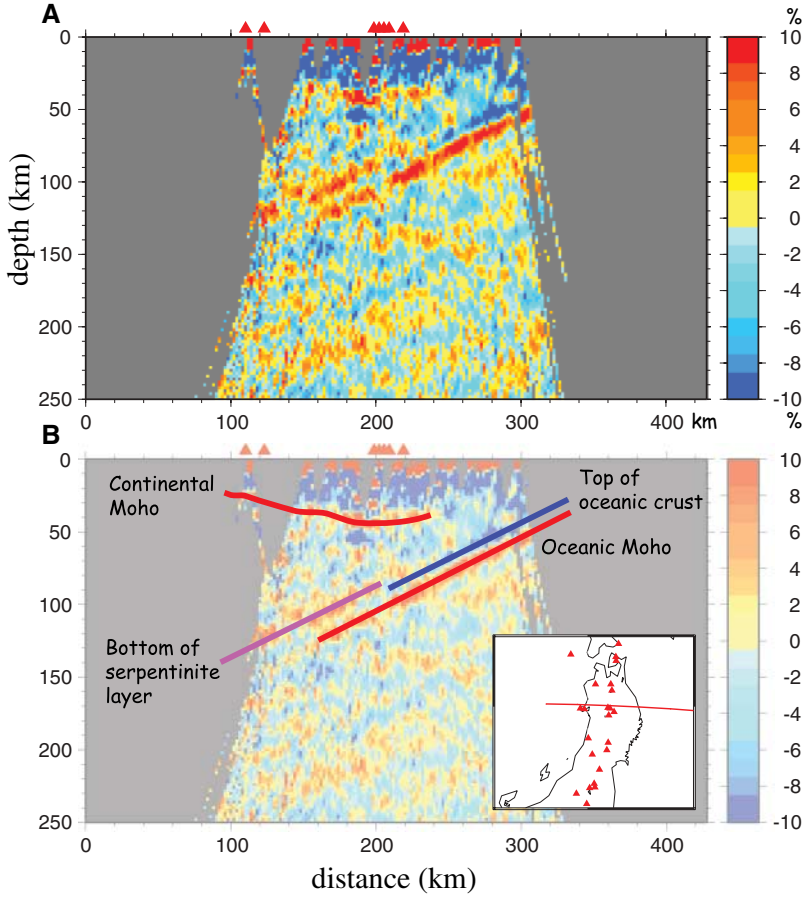

Fig. 1. The reflectivity profile beneath northeast Japan. (**A**) Reflectivities given by RFs are measures of local *S*-wave velocity jumps, because a *P*-to-*S* seismic wave conversion is sensitive to the *S*-wave velocity change. Red and blue colors correspond to velocity increase and decrease with depth, respectively. The color scale is given in terms of an equivalent *S*-wave velocity change (in percent) at a first-order discontinuity. (**B**) Interpretation of the image is overlaid on top of the reflectivity profile in (A). The continental Moho is not imaged well because of the frequency range used for the analysis. (Inset) A map of northeast Japan. The red line delineates where the 100-km-wide cross section is made. Red triangles indicate volcanoes active in the past 10,000 years (Smithsonian Institution, Global Volcanism Program) and are also plotted on the top of the cross sections.

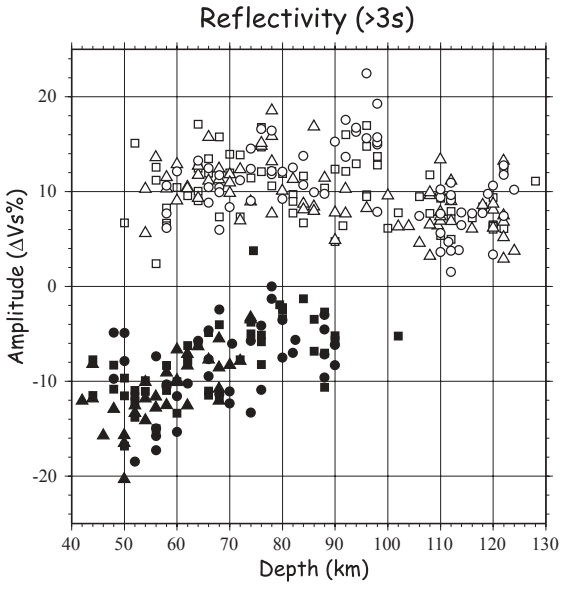

Fig. 2. Amplitude variation of the imaged reflectivity peaks. Peak values of the reflectivities of the interpreted images (along the red and blue lines in Fig. 1B) of three sections (Fig. 1A and fig. S1, D and F) are shown as a function of depth. Open and closed symbols correspond to the red and blue images, respectively, in Fig. 1. The reflectivity values are given in terms of the equivalent *S*-wave velocity increase. The amplitude (or magnitude) of the negative reflectivities decreases with depth, whereas that of the positive ones stays almost constant down to a depth of ~100 km and then becomes weak. A low velocity of ~13% is consistent with the existence of a fully hydrated oceanic crust (blueschist) (*29*).

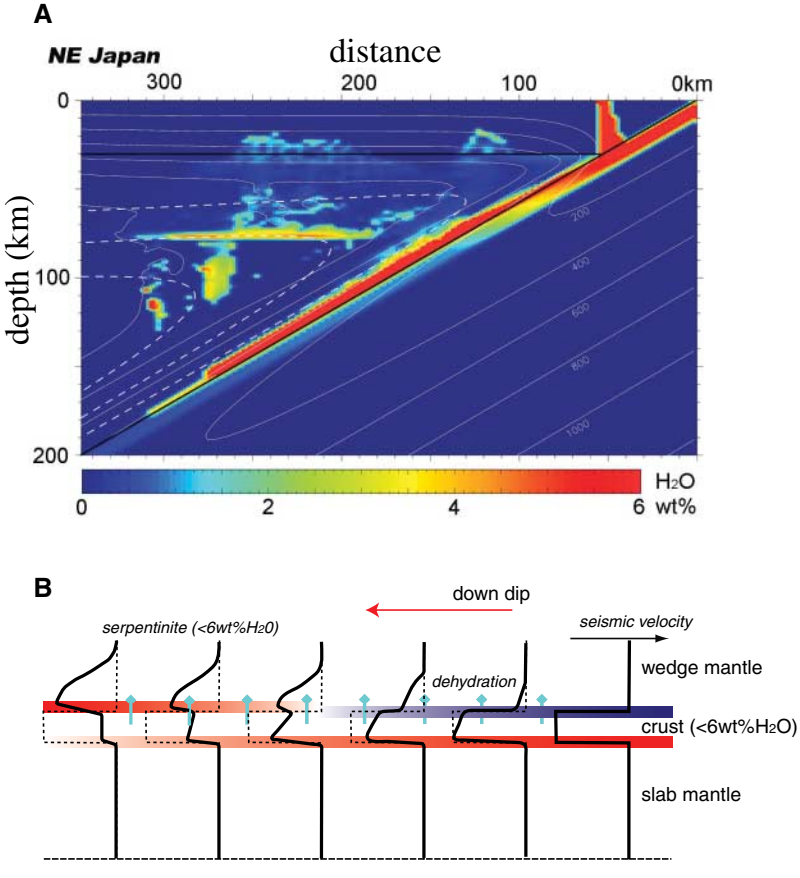

Fig. 3. Interpretation of the reflectivity profile in terms of the water transportation in the mantle wedge. (**A**) A numerical simulation of the water transportation beneath northeast Japan (*4*). Bright colors indicate a high concentration of water. The water in the hydrated oceanic crust [shallow (<50 km) dipping red layer] is expelled to serpentinize the mantle wedge, which is dragged downward on top of the subducting plate to form a serpentinite layer (deeper dipping red layer). (**B**) A schematic model for the effect of crustal dehydration on the seismic velocity near the top of the subducting plate. Seismic-velocity profiles (black lines) perpendicular to the slab surface are given at different down-dip distances. Red and blue colors show the expected reflectivities in a manner similar to that for the reflectivity profile (Fig. 1). Light blue arrows indicate the dehydration process. The slab surface is rotated to become horizontal.

The accurate relative location of RF images to seismicity and tomographic images of the same region is essential for our interpretation, but the RF image (Fig. 1) does not allow such a direct comparison because the effect of the dipping interface dislocates the image. Instead, we use a dip-corrected RF image (see SOM) for such a comparison (Fig. 4A). Two important observations may be made. First, most of the earthquakes in the upper plane of the double seismic zone are located above or near the peak of the positive RFs, and thus occur in the oceanic crust (or near the oceanic Moho); second, the positive RFs interpreted as the bottom of the serpentinite layer are located substantially deeper than the strong low-velocity region in the mantle wedge, which apparently corresponds to the melt pathway for the arc volcanism (*8*), and thus are unlikely to be directly related to this feature.

The presence of a low-velocity layer near the top part of the subducting plate has been observed in some subduction zones (*15*, *16*, *23*–*25*) and often interpreted as a subducted hydrated oceanic crust (*13*, *15*). Our observation sheds new light on how we interpret those low-velocity structures. Assuming that the amount of water roughly determines the seismic-velocity reduction in both crust and mantle and that most of the expelled water serpentinizes the mantle, the depth at which the top of the oceanic crust loses its illumination may roughly correspond to a depth at which about half of the water in the crust is dehydrated [completion of blueschist dehydration (*14*), ~90-km depth]. As the dehydration continues further, the oceanic Moho also loses its illumination (~125-km depth), indicating that most of the water in the oceanic crust is dehydrated. Below this depth, the bottom of the serpentinite layer dominates the reflectivity profile until the depth at which serpentine itself becomes unstable, thereby releasing water upward to trigger melting in the wedge (*4*) (130- to 150-km depth, Fig. 4). If the temperature of this region is cold enough, another hydrous mineral, phase-A, may further bring water down to a depth greater than 300 km (*4*); this phase-A layer on the top of the slab should show a velocity profile similar to that of the serpentinite layer in Fig. 3B, except that the signature is weaker after the serpentine dehydration. Such a structure had been observed in the deeper portion (250- to 400-km depth) beneath central Japan (*23*) as a sharp velocity increase at the top surface of the subducting slab. This feature was originally attributed to the partial melting of the wedge mantle (*23*) and, more recently, to the low-velocity due to the oceanic crust (*15*). In the context of the present work, we attribute it to the hydrated mantle wedge as a continuation of the serpentinite layer, as suggested above. Furumura and Kennett (*26*) recently showed that the suggested persistent deep (100 to 250 km) low-velocity crustal layer (*15*, *24*) is not required from seismic waveform data beneath Japan. Indeed, a reflectivity profile

corresponding to a velocity increase subparallel to the deep-slab seismicity is observed down to ~400 km, just above the 410-km discontinuity beneath central Japan (*27*). The schematic model (Fig. 4B) is qualitatively consistent with most of the seismic observations so far made beneath northeast and central Japan (*15*, *23*, *26*, *28*) and may possibly explain the depth variation of the reflectivity at the slab surface (*13*). It brings many individual observations together in a single framework that is consistent with petrological (*1*) and geodynamical (*4*, *14*, *17*) arguments. Thus, our result provides convincing seismic evidence to delineate how water is transported into the deep mantle within the mantle wedge in a cold subduction environment.

The amplitudes of the reflectivity profile of both sides of the oceanic crust at shallow depths (~50 km) are large and consistent with the existence of a fully hydrated oceanic crust (Fig. 2) that may contain ~6 weight % H_2O (*4*, *14*). To produce the RF signature corresponding to the bottom of the serpentinite layer as observed (Fig. 1), a large amount of the water expelled from the oceanic crust by dehydration must be used to serpentinize the wedge mantle. Consequently, a substantial amount (several wt %) of water must be transported to depths of ~130 to 150 km through this channel. How much deeper and how much water is transported through this channel are important questions that must be answered to quantify the water circulation budget in the subduction zone. Waveform analyses of broadband data of reflected and converted waves at the top of the slab below ~150-km depth may provide answers to these questions, eventually allowing us to estimate the overall water circulation budget in the Earth system (*4*).

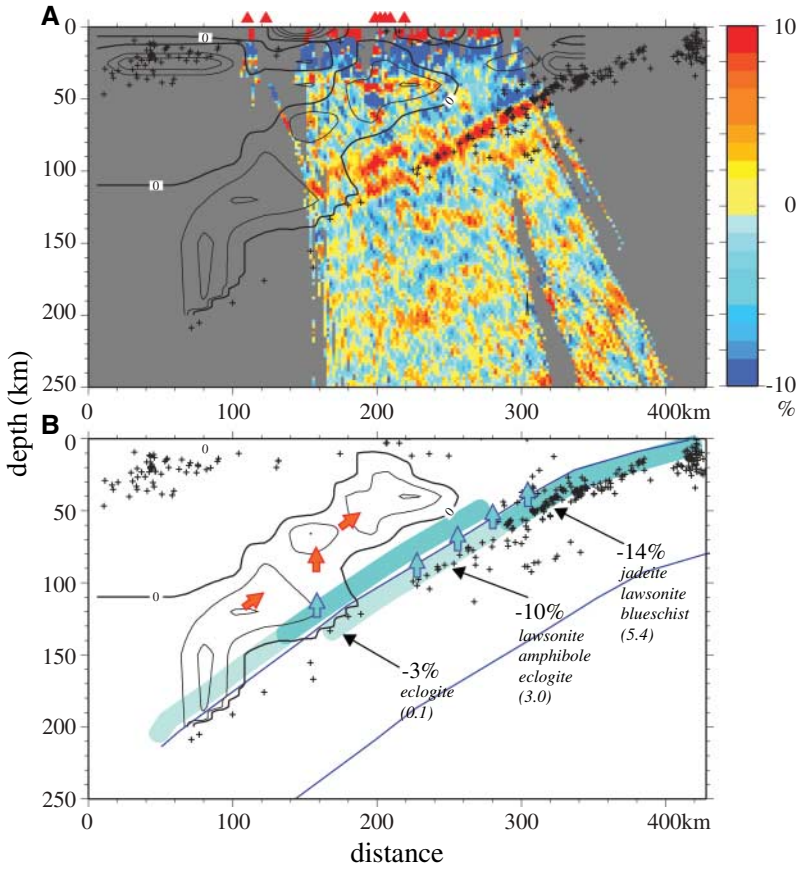

Fig. 4. Integrated seismic images beneath the Tohoku subduction zone and a schematic model for the water transportation. (**A**) The dip-corrected reflectivity image of Fig. 1A is compared with the tomographic image (*7*) and the seismicity (magnitude larger than 3) reported by the Japan Meteorological Agency. The *S*-wave tomographic image above the subducting slab is given by contours with 3% velocity-change intervals. The thick solid contours give the average velocity. Thin contours in the mantle wedge correspond to the low-velocity regions. Plus signs indicate earthquakes. Red triangles are the same as in Fig. 1. (**B**) The pathway of water transportation postulated by Iwamori [(*4*); see also (*30*)] is schematically illustrated by light blue and red colors for nonmagmatic and magmatic paths, respectively. Negative percentages give the *S*-wave velocities of fully hydrated oceanic crust relative to those of the slab-mantle estimated by Hacker and Abers (*29*) (also given are the names of the stable crustal rock facies, and wt % H_2O in parentheses). The plate boundaries of the subducting slab are shown schematically as blue lines. Earthquakes and contours of the low-velocity region in the mantle wedge of Fig. 4A are also shown.

References and Notes

1. Y. Tatsumi, *J. Geophys. Res.* **94**, 4697 (1989).
2. M. E. Magee, M. D. Zoback, *Geology* **21**, 809 (1993).
3. S. Karato, in *Geophys. Monogr. 138* (American Geophysical Union, Washington, DC, 2003), pp. 135–152.
4. H. Iwamori, *Chem. Geol.* **239**, 182 (2007).
5. A. Hasegawa, N. Umino, A. Takagi, *Tectonophysics* **47**, 43 (1978).
6. D. Zhao, A. Hasegawa, S. Horiuchi, *J. Geophys. Res.* **97**, 19909 (1992).
7. J. Nakajima, T. Matsuzawa, A. Hasegawa, D. Zhao, *J. Geophys. Res.* **106**, 21843 (2001).
8. J. Nakajima, Y. Takei, A. Hasegawa, *Earth Planet. Sci. Lett.* **234**, 59 (2005).
9. Y. Tamura, Y. Tatsumi, D. Zhao, Y. Kido, H. Shukuno. *Earth Planet. Sci. Lett.* **197**, 105 (2002).
10. S. Honda, T. Yoshida, *Geochem. Geophys. Geosyst.* **6**, Q01002 10.1029/2004GC000785 (2005).
11. J. Nakajima, A. Hasegawa, *Earth Planet. Sci. Lett.* **225**, 365 (2004).
12. S. M. Peacock, *Geol. Soc. Am. Bull.* **105**, 684 (1993).
13. G. R. Helffrich, in *Geophys. Monogr. 96* (American Geophysical Union, Washington, DC, 1996), pp. 215–222.
14. B. R. Hacker, S. M. Peacock, G. A. Abers, S. D. Holloway, *J. Geophys. Res.* **108**, 2030 10.1029/2001JB001129 (2003).
15. T. Matsuzawa, N. Umino, A. Hasegawa, A. Takagi, *Geophys. J. R. Astron. Soc.* **86**, 767 (1986).
16. X. Yuan *et al.*, *Nature* **408**, 958 (2000).
17. H. Iwamori, D. Zhao, *Geophys. Res. Lett.* **27**, 425 (2000).
18. L. P. Vinnik, *Phys. Earth Planet. Int.* **15**, 39 (1977).
19. C. A. Langston, *J. Geophys. Res.* **84**, 4749 (1979).
20. C. J. Ammon, *Bull. Seismol. Soc. Am.* **81**, 2504 (1991).
21. K. Obara, K. Kasahara, S. Hori, Y. Okada, *Rev. Sci. Instrum.* **76**, 021301 10.1063/1.1854197 (2005).
22. The bottom of the serpentinite layer appears to be also slightly diffusive because it is not resolved in the higher-frequency image (SOM). If serpentinization of the mantle peridotite occurs in an equilibrium manner, this boundary may be expected to be sharp. Our result, however, does not support this scenario. The detailed mechanism of water transportation in the mantle wedge is poorly known, and some additional factor appears to be necessary to fully explain our observation.
23. H. Okada, *J. Phys. Earth* **27** (suppl.), S53 (1979).
24. G. A. Abers, *Earth Planet. Sci. Lett.* **176**, 323 (2000).
25. A. Ferris, G. A. Abers, D. H. Christensen, E. Veenstra, *Earth Planet. Sci. Lett.* **214**, 575 (2003).
26. T. Furumura, B. L. N. Kennett, *J. Geophys. Res.* **110**, B10302 (2005).
27. H. Kawakatsu, S. Watada, *EOS Trans. AGU* **86** (Fall Meet. Suppl.), abstract DI41A (2005).
28. S. Kita, J. Nakajima, T. Matsuzawa, A. Hasegawa, *Geophys. Res. Lett.* **33**, L24310 (2006).
29. B. R. Hacker, G. A. Abers, *Geochem. Geophys. Geosyst.* **5**, Q01005 (2004).
30. A. Hasegawa, J. Nakajima, in *Geophys. Monogr.* **150** (American Geophysical Union, Washington, DC, 2004), pp. 81–94.

31. We thank H. Iwamori and C. Bina for discussions and J. Nakajima for the tomographic model. An anonymous reviewer provided useful comments. This research was supported by the Japan Society for the Promotion of Science and by the Ministry of Education, Culture, Sports, Science and Technology of Japan.

Supporting Online Material

www.sciencemag.org/cgi/content/full/316/5830/1468/DC1
SOM Text
Fig. S1
References

5 February 2007; accepted 12 April 2007
10.1126/science.1140855